Journal of Geophysical Research: Biogeosciences

RESEARCH ARTICLE
10.1029/2018JG004401

Attribution of Local Temperature Response to Deforestation

Weilin Liao[1,2], **Angela J. Rigden**[3], **and Dan Li**[2]

[1]School of Geography and Planning, Sun Yat-sen University, Guangzhou, China, [2]Department of Earth and Environment, Boston University, Boston, MA, USA, [3]Department of Earth and Planetary Sciences, Harvard University, Cambridge, MA, USA

Key Points:
- Land surface temperature response to deforestation is attributed to different biophysical changes using two attribution methods
- Similarity and dissimilarity between the attribution results from the two methods are identified
- Acceptable agreement between observed and modeled land surface temperature change is the prerequisite for attribution

Supporting Information:
- Supporting Information S1

Correspondence to:
D. Li,
lidan@bu.edu

Citation:
Liao, W., Rigden, A. J., & Li, D. (2018). Attribution of local temperature response to deforestation. *Journal of Geophysical Research: Biogeosciences*, *123*. https://doi.org/10.1029/2018JG004401

Received 15 JAN 2018
Accepted 10 APR 2018
Accepted article online 24 APR 2018

Abstract Land use and land cover change such as deforestation can directly induce changes in land surface temperature (LST). Using observational data from four paired eddy covariance sites, we attribute changes in LST induced by deforestation to changes in radiation, aerodynamic resistance, the Bowen ratio or surface resistance, and heat storage using two different methods: the intrinsic biophysical mechanism (IBM) method and the two-resistance mechanism method. The two models are first optimized to reduce the root-mean-square error of the simulated daily LST change by using daily-averaged inputs and a weighted average approach for computing the sensitivities. Both methods indicate that the daytime warming effect of deforestation is mostly induced by changes in aerodynamic resistance as the surface becomes smoother after deforestation, and the nighttime cooling effect of deforestation is controlled by changes in aerodynamic resistance, surface resistance, radiation, and heat storage. Both methods also indicate that changes in atmospheric temperature have a large impact on LST and need to be included in the LST attribution. However, there are significant differences between the two methods. The IBM method tends to overestimate the contribution of aerodynamic resistance due to the assumption that aerodynamic resistance and the Bowen ratio are independent. Additionally, the IBM method underestimates the contributions of radiation and heat storage during the daytime but overestimates them at night. By highlighting the similarity and dissimilarity between the two methods, this study suggests that acceptable agreement between observed and modeled LST change is the prerequisite for attribution but does not guarantee correct attribution.

1. Introduction

The Fifth Assessment Report of the Intergovernmental Panel on Climate Change states that compared with changes of natural forcing (i.e., solar variability and volcanoes) and modes of internal variability, more than half of the increase in global mean surface temperature is very likely induced by the increase of anthropogenic forcing in the past few decades (Intergovernmental Panel on Climate Change, 2013). In addition to the increasing greenhouse gas emissions, land use and land cover change (LULCC) such as deforestation is an important anthropogenic forcing to global climate change (Alkama & Cescatti, 2016; Bonan, 2008; Feddema et al., 2005; Mahmood et al., 2014; Runyan et al., 2012). Based on global satellite observations, Li et al. (2015) found that LULCC from forest to open land induced strong daily warming of 2.4 ± 0.10°C in the tropics, followed by 0.97 ± 0.07°C in the southern hemisphere and 0.27 ± 0.03°C in the northern hemisphere. Global simulations of the impact of LULCC showed that deforestation can cause surface temperature increases up to 2°C in the tropics (Defries et al., 2002; Feddema et al., 2005).

LULCC can rapidly alter land surface properties and states such as surface albedo, surface roughness, soil moisture, and heat storage (Pielke et al., 2011). These changes directly affect land surface temperature (LST) through changes in energy, water, and momentum fluxes (Bonan, 2008; Bright et al., 2015). Quantifying the contributions of these different biophysical effects to changes in LST is of much interest to the academic community as it improves our understanding of the impacts of LULCC on the local climate. It is also important for policy makers and planners because it can inform the design of warming mitigation strategies. There are two well-known changes associated with deforestation that have competing temperature effects through altering the surface energy budget: the increase in albedo that leads to the decrease in absorbed shortwave radiation and the decrease in evapotranspiration (Li et al., 2015). The first process (related to albedo) tends to dominate in high-latitude regions, resulting in a cooling effect of deforestation. The second process (related to evapotranspiration) tends to dominate in the tropics, resulting in a warming effect of deforestation. The competition between the two processes produces the latitudinal dependence of temperature effects of deforestation (Davin & De Noblet-Ducoudre, 2010; Lee et al., 2011; Li et al., 2016). Their

relative importance, which determines whether deforestation has a net cooling or warming effect, remains controversial in the temperate midlatitudes (Findell et al., 2017; Li et al., 2015).

To quantitatively attribute changes in LST to biophysical changes induced by LULCC, many surface energy balance-based methods have been proposed (Burakowski et al., 2017; Chen & Dirmeyer, 2016; Lee et al., 2011; Luyssaert et al., 2014; Zhao, Lee, & Schultz, 2017). Luyssaert et al. (2014) attributed changes in LST due to LULCC to changes in surface albedo, incoming radiation, sensible heat flux, latent heat flux, and ground heat flux using observed fluxes. In this model, while changes in the albedo associated with deforestation are fairly straightforward to consider, changes in evapotranspiration cannot be traced to changes in biophysical factors such as surface roughness and evaporation efficiency (Davin & De Noblet-Ducoudre, 2010). A method proposed by Juang et al. (2007) attributes changes in LST to changes in albedo, emissivity, ground heat flux, and a parameter that lumps the effects of aerodynamic resistance and the Priestley-Taylor coefficient (Priestley & Taylor, 1972) in the parameterization of evaporation. Their method does not explicitly separate the effects of surface roughness and evaporation efficiency, both of which affect LST. Notably, Lee et al. (2011) proposed the intrinsic biophysical mechanism (IBM) method, which attributes changes in LST to changes in radiative forcing, aerodynamic resistance (mainly depending on the surface roughness), and the Bowen ratio. Compared to previous methods, the IBM method separates the impact of surface roughness from the Bowen ratio, which is of particular importance for developing warming mitigation strategies (Zhao, Lee, & Schultz, 2017). Using the IBM method and eddy-covariance data from paired sites, several studies showed that changes in aerodynamic resistance induced by deforestation are the dominant driver of LST changes in both daytime and nighttime over midlatitude regions (Burakowski et al., 2017; Chen & Dirmeyer, 2016; Lee et al., 2011). The IBM method has also been widely used to attribute LST changes induced by urbanization (Cao et al., 2016; Zhao et al., 2014).

To quantify the contribution of different biophysical factors to LST changes, models should ensure that the attributing variables are independent of one another. Recently, Rigden and Li (2017) pointed out that the IBM method assumes that the aerodynamic resistance and the Bowen ratio are independent of each other. Hereafter this assumption is referred to as the "independence assumption." Using eddy covariance data from 75 sites within the AmeriFlux network, they demonstrated that this independence assumption invoked by the IBM method may lead to an overestimation of the contribution of the aerodynamic resistance by 10–25%. To avoid this assumption, Rigden and Li (2017) proposed the two-resistance mechanism (TRM) method, which uses the aerodynamic resistance and the surface resistance (mainly controlled by soil moisture and vegetation properties) rather than the Bowen ratio as in the IBM method to parameterize latent heat flux. The role of surface resistance in controlling evapotranspiration and thus LST is similar to that of evaporation efficiency, which was explored by Davin and De Noblet-Ducoudre (2010) using sensitivity simulations with a global climate model.

While Rigden and Li (2017) demonstrated that the IBM method tends to overestimate the contribution of the aerodynamic resistance, the differences between the IBM and TRM methods in terms of contributions from radiation and heat storage terms were not examined. In addition, they did not directly report the performance of the two methods in capturing LST changes induced by LULCC because they did not use data from paired sites. In this study, we select four paired sites from the AmeriFlux network to conduct a detailed comparison between the two methods. Additionally, we also investigate the models' sensitivity to the temporal scale of input variables, as well as strategies to increase the models' performance in capturing LST changes. The paper is organized as follow: section 2 describes the observational data, the two attribution models used in this study, and the application and training of the two models; section 3 presents the results and discusses the similarity and dissimilarity in the attribution results from the two methods; and section 4 concludes the study.

2. Materials and Methods

2.1. Observational Data

We obtain the eddy covariance and meteorological data from the AmeriFlux data repository (http://ameriflux.lbl.gov) and process the data following Rigden and Salvucci (2015). To explore the biophysical impacts of LULCC on LST, we select four pairs of flux towers from the AmeriFlux network with half-hourly measurements that last at least one year for both sites (Table 1). For each pair, one flux tower is located over open land

Table 1
Description of the Four Paired Sites From AmeriFlux Network

Pair ID	Site name	AmeriFlux	Reference with site description	Latitude	Longitude	Land cover type	Annual precipitation (mm)	Separation (km)	Period analyzed
1	Duke Forest Open Field	US-Dk1	Oishi, Novick, and Stoy (2016a), doi:10.17190/AMF/1246046	35.971	−79.093	Grasslands	678.8	0.68	2001–2006
	Duke Forest Hardwoods	US-Dk2	Oishi, Novick, and Stoy (2016b), doi:10.17190/AMF/1246083	35.974	−79.100	Deciduous broadleaf forests	678.8		
2	Duke Forest Open Field	US-Dk1	Oishi et al. (2016a), doi:10.17190/AMF/1246046	35.971	−79.093	Grasslands	678.8	0.78	2001–2006
	Duke Forest Loblolly Pine	US-Dk3	Oishi, Novick, and Stoy (2016c), doi:10.17190/AMF/1246048	35.978	−79.094	Evergreen needleleaf forests	757.0		
3	North Carolina Clearcut	US-NC1	Noormets (2016a), doi:10.17190/AMF/1246082	35.812	−76.712	Open shrublands	822.2	4.03	2005–2009
	North Carolina Loblolly	US-NC2	Noormets (2016b), doi:10.17190/AMF/1246083	35.803	−76.668	Evergreen needleleaf forests	904.6		
4	Flagstaff Wildfire	US-Fwf	Dore and Kolb (2016b), doi:10.17190/AMF/1246052	35.445	−111.772	Grasslands	450.7	33.84	2005–2010
	Flagstaff Managed Forest	US-Fmf	Dore and Kolb (2016a), doi:10.17190/AMF/1246050	35.143	−111.727	Evergreen needleleaf forests	324.7		

(grassland or open shrubland) and the other is located over forest (deciduous broadleaf forest or evergreen needleleaf forest). Note that pairs 1 and 2 share the same open land tower. In our analysis, the forest is regarded as the reference state, and the open land is regarded as a perturbation to this reference state. Therefore, these cases represent the impacts of deforestation on local LST. The four paired sites are located in midlatitudes (~36°N). The first three paired sites are located in temperate regions with annual average precipitation greater than 670 mm, while pair 4 is in an arid region with annual average precipitation less than 450 mm. However, snow cover at Flagstaff sites (pair 4) is more frequent compared to the other three paired sites, which are all in North Carolina. This has important implications for the attribution results in the winter season.

Figure 1 shows the summer averaged diurnal cycles of the four radiative fluxes, sensible heat flux, and latent heat flux over the forest site and the open land site of pair 1. Although the diurnal cycle of the incoming shortwave radiation is similar between the open land and forest, the other fluxes differ substantially. For instance, more shortwave radiation is reflected at the open land site during daytime, reflecting the higher albedo of the open land than the forest. Also, more longwave radiation is emitted at the open land site during daytime, reflecting the higher LST of the open land than the forest. Additionally, the sensible heat flux over open land is larger than that over forest, while the latent heat flux over open land is smaller. Together these differences in the observed radiative and turbulent fluxes are caused by the contrasting surface properties between the two land cover types, including the surface albedo, soil moisture, heat storage, and surface roughness, and result in different LSTs (Rotenberg & Yakir, 2011). In the following, we use two methods (the IBM method and TRM method) to attribute the LST changes induced by deforestation to changes in different biophysical factors and evaluate the differences between the IBM and TRM methods. The details about the two methods are presented in the next section.

2.2. Attribution Methods

The IBM and TRM methods are both based on the surface energy balance equation:

$$R_n = S_{\text{in}}(1-\alpha) + \varepsilon L_{\text{in}} - \varepsilon\sigma T_s^4 = H + LE + G \tag{1}$$

where R_n is the net surface radiation, S_{in} is the incoming shortwave radiation, L_{in} is the incoming longwave radiation, α is the surface albedo, ε is the surface emissivity, σ is the Stephan-Boltzmann constant, T_s is the LST, H is the sensible heat flux, LE is the latent heat flux, and G is the heat storage. In this study, G is

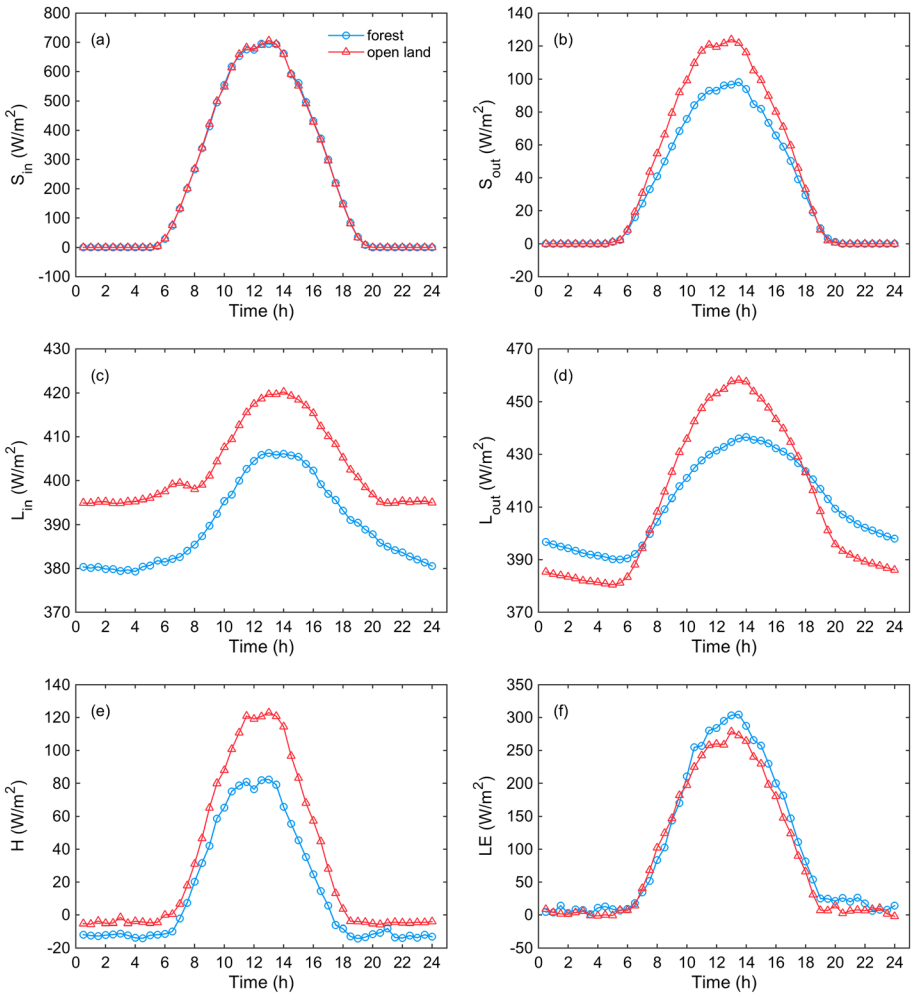

Figure 1. The averaged diurnal cycles of (a) incoming shortwave radiation (S_{in}), (b) outgoing shortwave radiation (S_{out}), (c) incoming longwave radiation (L_{in}), (d) outgoing longwave radiation (L_{out}), (e) sensible heat flux (H), and (f) latent heat flux (LE) over the forest (deciduous broadleaf, US-DK2) site and the open land (grassland, US-DK1) site of pair 1 in summer.

estimated as the residual of the surface energy balance equation. In both methods, the sensible heat flux is parameterized using the resistance concept (Monteith & Unsworth, 1990), as follows:

$$H = \frac{\rho c_p}{r_a}(T_s - T_a) \tag{2}$$

where ρ is the air density, c_p is the specific heat of air at constant pressure, r_a is the aerodynamic resistance, and T_a is the air temperature. Unlike the sensible heat flux, the latent heat flux is parameterized differently in the two methods. The IBM method uses the sensible heat flux and the Bowen ratio ($\beta = H/LE$) to parameterize the latent heat flux, while the TRM method uses the aerodynamic resistance and the surface resistance (r_s) to parameterize the latent heat flux.

2.2.1. The Intrinsic Biophysical Mechanism (IBM) Method

In the IBM method, the latent heat flux is given as

$$LE = \frac{H}{\beta} \tag{3}$$

Linearizing the outgoing longwave radiation term in equation (1) based on the Taylor series expansion and making use of equations (2) and (3), a revised surface energy balance equation can be written as

$$S_{in}(1-\alpha) + \varepsilon L_{in} - \varepsilon\sigma T_a^4 - 4\varepsilon\sigma T_a^3(T_s - T_a) = \frac{\rho c_p}{r_a}(T_s - T_a) + \frac{\rho c_p}{r_a \beta}(T_s - T_a) + G \tag{4}$$

Defining $R_n^* = S_{\text{in}}(1-\alpha) + \varepsilon L_{\text{in}} - \varepsilon\sigma T_a^4$ and $\lambda_o = 1/\left(4\varepsilon\sigma T_a^3\right)$, T_s can be solved from equation (4) as

$$T_s = \frac{\lambda_o\left(R_n^* - G\right)}{1 + \frac{\rho c_p \lambda_o}{r_a}\left(1 + \frac{1}{\beta}\right)} + T_a \tag{5}$$

To further simplify equation (5), we define $r_o = \rho c_p \lambda_o$ and $f_{\text{IBM}} = \frac{r_o}{r_a}\left(1 + \frac{1}{\beta}\right)$, leading to

$$T_s = \frac{\lambda_o\left(R_n^* - G\right)}{1 + f_{\text{IBM}}} + T_a \tag{6}$$

With the above equation for T_s, the LST change from forest to open land (ΔT_s, where Δ represents the change induced by LULCC) can be expressed as

$$\Delta T_s = (T_s)^{\text{open land}} - (T_s)^{\text{forest}} = \left[\frac{\lambda_o\left(R_n^* - G\right)}{1 + f_{\text{IBM}}}\right]^{\text{open land}} - \left[\frac{\lambda_o\left(R_n^* - G\right)}{1 + f_{\text{IBM}}}\right]^{\text{forest}} + (T_a)^{\text{open land}} - (T_a)^{\text{forest}} \tag{7}$$

Expanding the right-hand side of the equation (7) around the reference (i.e., forest) state, ΔT_s can be attributed to changes in the radiative forcing, aerodynamic resistance, Bowen ratio, and land-atmosphere feedbacks, following:

$$(\Delta T_s)^{\text{IBM}} = \left(\frac{\partial T_s}{\partial R_n^*}\right)^{\text{IBM}}\left(\Delta R_n^* - \Delta G\right) + \left(\frac{\partial T_s}{\partial r_a}\right)^{\text{IBM}}\Delta r_a + \left(\frac{\partial T_s}{\partial \beta}\right)^{\text{IBM}}\Delta\beta + \Delta T_a \tag{8}$$

$$\left(\frac{\partial T_s}{\partial R_n^*}\right)^{\text{IBM}} = \frac{\lambda_o}{1 + f_{\text{IBM}}} \tag{9}$$

$$\left(\frac{\partial T_s}{\partial r_a}\right)^{\text{IBM}} = \frac{\lambda_o\left(R_n^* - G\right)}{\left(1 + f_{\text{IBM}}\right)^2}\frac{r_o}{r_a{}^2}\left(1 + \frac{1}{\beta}\right) \tag{10}$$

$$\left(\frac{\partial T_s}{\partial \beta}\right)^{\text{IBM}} = \frac{\lambda_o\left(R_n^* - G\right)}{\left(1 + f_{\text{IBM}}\right)^2}\frac{r_o}{r_a\beta^2} \tag{11}$$

The subscript and superscript "IBM" indicate the IBM method. The f_{IBM} is called the energy redistribution factor, and R_n^* is the apparent net radiation defined based on air temperature instead of LST. When the energy redistribution factor is positive, the higher the f_{IBM}, the lower the sensitivity of LST to radiative forcing (Lee et al., 2011) and the more important nonradiative processes become in controlling LST changes (Bright et al., 2017).

Note that equation (8) retains only the first-order terms in the Taylor series expansion. This has two important implications to consider. First, it implicitly assumes that changes in the attributing variables (e.g., Δr_a and $\Delta\beta$) are independent of each other, as discussed in Rigden and Li (2017). Second, while the Taylor series expansion requires the partial derivatives (i.e., the sensitivities) to be estimated at the reference state, in reality this might introduce large errors because the perturbations are not small enough. This effect will be explicitly investigated later.

Overall, it is clear that in the IBM method, the LST change due to deforestation is attributed to the changes in albedo (or net radiation), aerodynamic resistance, Bowen ratio, heat storage, and atmospheric feedbacks. Different from the IBM method used in Lee et al. (2011), in this study we also consider the changes in atmospheric temperature (ΔT_a). This is because, although the paired sites are relatively close to each other, they may not share the same background meteorological conditions (Chen & Dirmeyer, 2016).

2.2.2. The Two-Resistance Mechanism (TRM) Method

Different from the IBM method, the latent heat flux in the TRM method is parameterized as (Monteith & Unsworth, 1990)

$$LE = \frac{\rho L_v}{(r_a + r_s)}\left(q_s^*(T_s) - q_a\right) \tag{12}$$

where L_v is the latent heat of vaporization, q_s^* is the saturated specific humidity at T_s, and q_a is the atmosphere specific humidity. Similar to the derivations in equations (4)–(11), the LST change can be attributed

to changes in the radiative forcing, aerodynamic resistance, surface resistance, and atmospheric feedback (Rigden & Li, 2017), following

$$(\Delta T_s)^{\mathrm{TRM}} = \left(\frac{\partial T_s}{\partial R_n^*}\right)^{\mathrm{TRM}} (\Delta R_n^* - \Delta G) + \left(\frac{\partial T_s}{\partial r_a}\right)^{\mathrm{TRM}} \Delta r_a + \left(\frac{\partial T_s}{\partial r_s}\right)^{\mathrm{TRM}} \Delta r_s + \Delta T_a \tag{13}$$

$$\left(\frac{\partial T_s}{\partial R_n^*}\right)^{\mathrm{TRM}} = \frac{\lambda_o}{1 + f_{\mathrm{TRM}}} \tag{14}$$

$$\left(\frac{\partial T_s}{\partial r_a}\right)^{\mathrm{TRM}} = \frac{\lambda_o \rho L_v \left(q_a^*(T_a) - q_a\right)}{\left(r_a + r_s\right)^2} \frac{1}{(1 + f_{\mathrm{TRM}})} + \lambda_o \left[R_n^* - G - \frac{\rho L_v \left(q_a^*(T_a) - q_a\right)}{(r_a + r_s)}\right] \frac{1}{(1 + f_{\mathrm{TRM}})^2} \frac{r_o}{r_a^2} \left[1 + \frac{\delta}{\gamma}\left(\frac{r_a}{r_a + r_s}\right)^2\right] \tag{15}$$

$$\left(\frac{\partial T_s}{\partial r_s}\right)^{\mathrm{TRM}} = \frac{\lambda_o \rho L_v \left(q_a^*(T_a) - q_a\right)}{\left(r_a + r_s\right)^2} \frac{1}{(1 + f_{\mathrm{TRM}})} + \lambda_o \left[R_n^* - G - \frac{\rho L_v \left(q_a^*(T_a) - q_a\right)}{(r_a + r_s)}\right] \frac{1}{(1 + f_{\mathrm{TRM}})^2} \frac{\delta}{\gamma} \frac{r_o}{(r_a + r_s)^2} \tag{16}$$

where $\delta = \left.\frac{\partial e^*}{\partial T}\right|_{T_a}$, $\gamma = \frac{c_p P}{0.622 L_v}$, e^* is the saturation vapor pressure, and P is the air pressure. Because of the difference in the parameterization of latent heat flux, the energy redistribution factor in the TRM method is different from that in the IBM method: $f_{\mathrm{TRM}} = \frac{r_o}{r_a}\left[1 + \frac{\delta}{\gamma}\left(\frac{r_a}{r_a + r_s}\right)\right]$. It is important to recognize that in addition to the differences in $\partial T_s/\partial r_a$ between the IBM and TRM methods as shown in Rigden and Li (2017), the sensitivity to radiative forcing and heat storage ($\partial T_s/\partial R_n^*$) is also different between the two methods due to the difference in the energy redistribution factor.

2.3. Application and Validation of the Two Attribution Methods

The required inputs of the IBM and TRM methods include the sensible heat flux, latent heat flux, LST, apparent net radiation, and air temperature for each land cover type. The TRM method also requires measurements of atmosphere specific humidity and air pressure. Other critical inputs such as the aerodynamic and surface resistances are inferred from observed variables such as sensible and latent heat fluxes (see equations (2) and (12)).

To estimate LST from the measurements of outgoing longwave radiation, we assume constant emissivity values of 0.92, 0.93, and 0.95 for grassland, deciduous broadleaf forest, and evergreen needleleaf forest, respectively (Tao et al., 2013). However, the emissivity of loblolly pine (evergreen needleleaf forest) at US-Dk3 is set to be 0.93 instead of 0.95. This is because if the emissivity of loblolly pine (evergreen needleleaf forest) at US-Dk3 was 0.95, nearly all ($T_s - T_a$) with T_s inferred from outgoing longwave radiation would have the opposite sign as the measured sensible heat flux during daytime in summer (Rigden, Li, & Salvucci, 2017), and the aerodynamic resistance would be negative and physically meaningless. This suggests that the emissivity value of 0.95 is probably too large for US-Dk3. As a result, we reduce the emissivity value of loblolly pine at US-Dk3 from 0.95 to 0.93 to ensure that there are enough valid data for the attribution analysis. We also perform a sensitivity analysis to examine the sensitivity of the attribution results to the emissivity value of grassland, which, according to Tao et al. (2013), ranges from 0.92 to 0.96 (see the supporting information). We find that while the inferred LSTs (and their changes) are sensitive to the emissivity value (Rigden et al., 2017), the conclusions about the attribution are not.

Prior to applying the IBM and TRM methods, we exclude half-hours with missing input data at any of the two sites. That is, the analysis is only conducted when data at both sites are available. We also exclude half-hours when the inferred aerodynamic resistance and/or surface resistance are negative. Furthermore, we separate the analysis into day and night according to the incoming shortwave radiation, as the impacts of deforestation on LST are different between daytime and nighttime (Li et al., 2015; Schultz et al., 2017). When the incoming shortwave radiation is larger than 25 W/m^2, the measurements are considered as daytime; otherwise, they are considered nighttime. Lastly, we only retain days or nights that have more than half of valid measurements.

Table 2
The Root-Mean-Square Errors (RMSEs) Between Observed and Modeled LST Changes for the IBM and TRM Methods

Pair ID	Method	Summer						Winter					
		Daytime			Nighttime			Daytime			Nighttime		
		m_{opt}	n	RMSE (°C)	m_{opt}	n	RMSE (°C)	m_{opt}	n	RMSE (°C)	m_{opt}	n	RMSE (°C)
1	IBM	1.2	8	0.10	5.5	6	1.71	0.7	93	0.40	0.1	14	0.61
	TRM	1.5	8	0.29	6.7	6	0.21	0.9	93	0.35	0.9	14	0.16
2	IBM	1	19	0.05	1.9	2	0.02	1.0	59	0.41	0.1	4	0.36
	TRM	0.9	19	0.18	2.2	2	0.13	1.2	59	0.25	1.0	4	0.11
3	IBM	1.0	139	0.05	2.3	69	1.71	0[a]	165	0.96	100[a]	89	0.58
	TRM	1.4	139	0.11	1.7	69	0.18	1.3	165	0.09	1.6	89	0.17
4	IBM	1.0	293	0.49	2.9	109	1.28	1.2	90	0.55	0.5	13	0.20
	TRM	1.9	293	0.86	1.2	109	0.58	1.4	90	0.16	0.5	13	0.24

Note. m_{opt} is the optimal value for m. n denotes the number of valid points used to attribution.
[a]In this study, we limit the range of m to be (0, 100). A value of 0 denotes that the partial derivative terms in the model are only determined with measurements at the reference (forest) site, while a value of 100 denotes that the partial derivative terms in the model are only calculated with measurements at the perturbed (open land) site.

Before presenting the results from the two attribution methods, it is critical to assess the performance of the two methods in capturing the observed ΔT_s. To do so, we use the root-mean-square error (RMSE) between the observed daily ΔT_s and the modeled daily ΔT_s (such that smaller RMSE values imply that the model better captures changes in LST). With half-hourly data, an immediate question is whether we should apply the models at the half-hourly scale and then aggregate the modeled ΔT_s to the daily scale, or apply the models at the daily scale by first aggregating the input variables. Since the attribution process is nonlinear for both IBM and TRM methods, the results may be sensitive to this choice. To investigate this in detail, we first compute the daytime ΔT_s during the summer at the half-hourly scale and then aggregate the daytime ΔT_s to daily scale. The resulting RMSE values between the observed ΔT_s and the modeled ΔT_s are quite large even when the ΔT_s is averaged to the daily scale, especially for pairs 2 and 4 (Figure S1). This is because there are many cases where the measured sensible and/or latent heat fluxes are close to zero at the half-hourly scale. In such conditions, the uncertainties in the inferred aerodynamic resistance, Bowen ratio, and surface resistance become large, which further result in large RMSEs for the modeled ΔT_s even when the ΔT_s is averaged to the daily scale. When we aggregate the input variables to daily scale and model the LST change at the daily scale, the RMSE values for the IBM and TRM methods decrease (Figure S2). These changes demonstrate that both models are sensitive to the temporal scale at which the attribution is conducted. Aggregating the input variables to daily scale effectively improves the accuracy of the models from the perspective of capturing the daily ΔT_s and is adopted in this paper.

While the RMSE values in Figure S2 seem acceptable for modeling LSTs, it is important to keep in mind that the attribution methods are designed to capture LST differences between forest and open land, rather than the LSTs themselves. In this sense, the RMSE values are still very large for pair 4 during the daytime in the summer (Figure S2) and the other paired sites during the nighttime in both the summer and winter (not shown). To further reduce the RMSEs, two strategies are adopted. First, we further exclude days when the absolute value of the daily sensible heat flux or latent heat flux is small (less than 1 W/m^2 for pairs 1 and 2 during nighttime in summer and 5 W/m^2 for others). This is again because when the measured sensible and latent heat fluxes are small, several inferred variables such as the aerodynamic and surface resistances become very uncertain, especially during nighttime. The exact threshold value is a compromise between removing outliers and maintaining a sufficient amount of data points for the attribution. Second, we introduce a weighted average approach to calculate the partial derivatives (e.g., $\partial T_s/\partial R_n^*$) in the models based on measurements at both sites, as follows:

$$X = \frac{X_{\text{forest}} + mX_{\text{open land}}}{1+m} \tag{17}$$

where X is the final partial derivative used in the model, m is average weight, and X_{forest} and $X_{\text{open land}}$ are the partial derivatives calculated only using data from the forest site and the open land site, respectively. It is

pointed out again that these partial derivatives are simply sensitivities of LST to changes in different biophysical factors. For example, $\partial T_s/\partial R_n^*$ is the sensitivity of LST to changes in net radiation. The rationale behind equation (17) is that perturbations from the forest state to the open land state are not small, and thus, only using data from the reference site to calculate the partial derivatives inevitably yields very large RMSE values even when we apply the model at the daily scale. We optimize the value of m by minimizing the RMSE for the IBM and TRM methods at the four-paired sites, respectively (Figure S3 and Table 2). As a result, the RMSE values for the two methods are further decreased at the four pairs (Figure 2). This is particularly the case for the nighttime results (Table 2). These findings suggest that the models' performances are sensitive to the calculation of the partial derivatives, which further anchors the point that LULCC induced perturbations on biophysical factors are not small.

Moreover, the two attribution methods are also sensitive to the energy balance closure. In addition to estimating G as the residual of the surface energy balance equation, we also use the original heat storage measurements as G and attribute LST changes without any energy balance correction. We find that the RMSE values are very large across all four pairs, suggesting that the two attribution methods do not apply to unbalanced energy flux data as expected. Overall, while the model formulation is fairly straightforward, the attribution is quite sensitive to the selected time scale, the calculation of the partial derivatives, and the energy balance closure. Before applying these attribution methods, it is crucial to ensure that the model adequately captures ΔT_s at the time scale that the attribution is conducted.

3. Results and Discussion

3.1. Response of LST to Deforestation

Based on the observational data, we attribute the LST change due to deforestation to changes in the radiative forcing, aerodynamic resistance, Bowen ratio (for the IBM method) or surface resistance (for the TRM method), and atmospheric feedback during daytime and nighttime in summer and winter, respectively. Furthermore, we also examine the impacts of the independence assumption in the IBM method by comparing the attribution results from the IBM method with those from the TRM method.

Figure 3 shows the observed and modeled LST changes due to deforestation during the daytime in summer, and the attribution based on the IBM and TRM methods, respectively. The modeled LST changes using the IBM and TRM methods both show good agreement with the observations, which is consistent with the results in Figure 2. Similar to the findings in previous studies (Chen & Dirmeyer, 2016; Li et al., 2015), deforestation has a warming effect on LST during the daytime in midlatitudes. The average LST increases by approximately 4°C at pair 4, 3°C at pairs 1 and 2, and 2°C at pair 3. In addition, the relative importance of different contributions is similar between the IBM and TRM methods. We note that the contribution from atmospheric feedbacks (T_a) is relatively large at pair 3, suggesting that the meteorological background has an important impact on local LST changes (Chen & Dirmeyer, 2016). When the impact of atmospheric feedback is not considered, the contribution from aerodynamic resistance becomes the dominant term. Forests are aerodynamically rougher and transfer heat more effectively than open land, thus experiencing lower LSTs than the open land during the daytime in summer (Burakowski et al., 2017; Chen & Dirmeyer, 2016; Lee et al., 2011; Rotenberg & Yakir, 2011). In addition to the difference in aerodynamic resistance, less evapotranspiration at open land leads to a warming effect of deforestation, whereas the larger albedo of open land leads to a cooling effect of deforestation during daytime in summer.

During nighttime in summer, the IBM and TRM methods can still capture the observed LST changes (Figure 4). However, contrary to the warming effect of deforestation in daytime, deforestation has a cooling effect on LST at night. The average LST decreases approximately by 1.5°C at pair 4, 1.0°C at pair 1 and pair 2, and 0.1°C at pair 3. Interestingly, the major drivers of LST change at night are different from the drivers in the day (Schultz et al., 2017). First of all, the atmospheric feedback have large contributions to the nighttime LST changes at all four pairs. Beyond the atmospheric feedback, the IBM and TRM methods show that there is no single dominant factor in the nighttime. Note that the number of observations at pairs 1 and 2 is smaller (6 for pair 1 and 2 for pair 2; Table 2) than those at pairs 3 and 4, which may affect the attribution results at pairs 1 and 2. Our results show that changes in radiation, heat storage, and surface resistance have large impacts on LST changes at night, which contradict the findings of Lee et al. (2011) and Chen and Dirmeyer (2016) that changes in aerodynamic resistance predominantly cause the nighttime cooling effect of

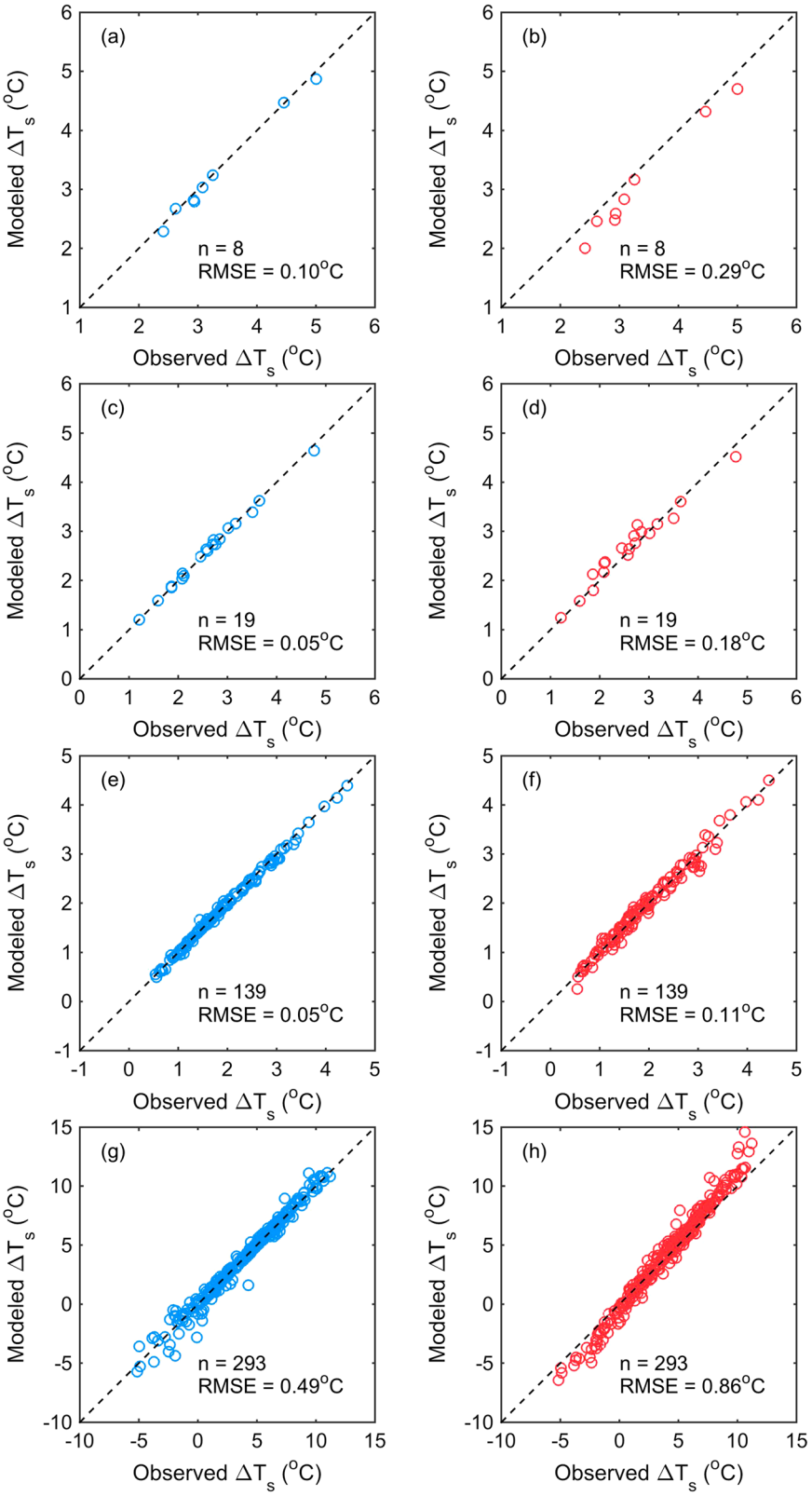

Figure 2. Comparisons between the observed ΔT_s and modeled ΔT_s during the daytime in summer at (a and b) pair 1, (c and d) pair 2, (e and f) pair 3, and (g and h) pair 4 when aggregating the input variables to the daily scale and using the optimal value of *m*. The left panels use the IBM method, and the right panels use the TRM method. RMSE donates the root-mean-square error between the observed ΔT_s and the modeled ΔT_s at the daily scale, while *n* denotes the number of valid points used to attribution. The dashed lines are 1:1 lines.

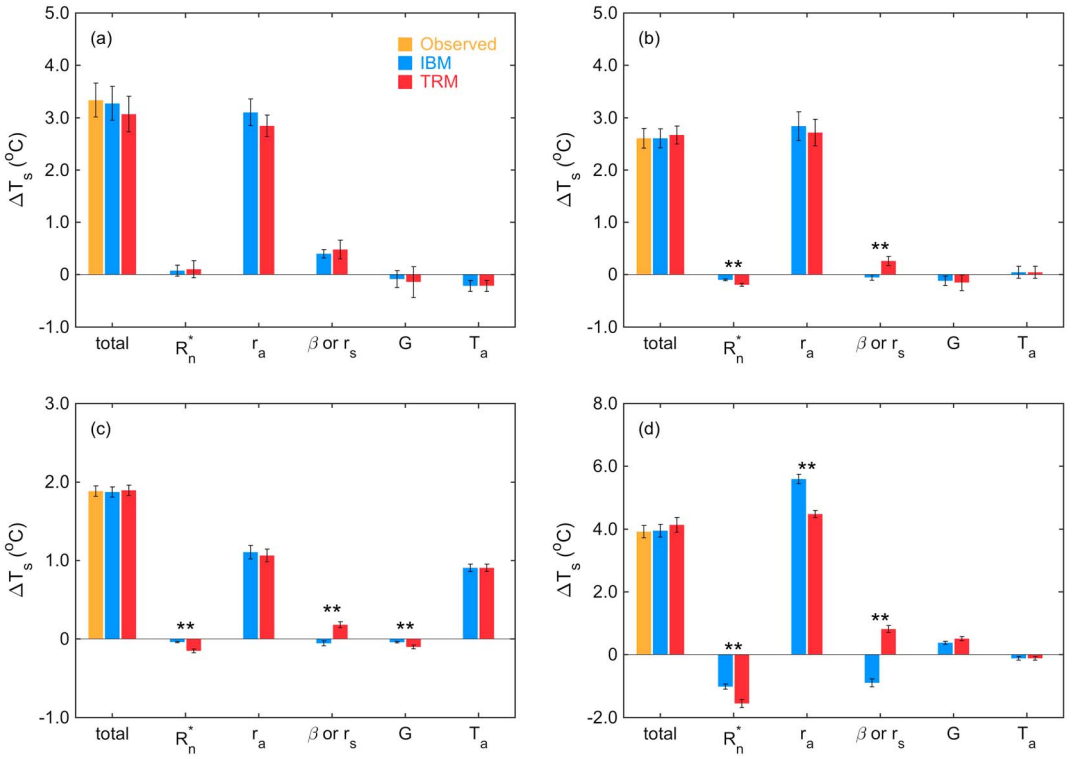

Figure 3. Attribution of land surface temperature changes due to deforestation during daytime in summer at (a) pair 1, (b) pair 2, (c) pair 3, and (d) pair 4. R_n^*, r_a, β or r_s, G, and T_a represent contributions from changes in radiation, aerodynamic resistance, Bowen ratio (for the IBM method) or surface resistance (for the TRM method), heat storage, and atmospheric feedback, respectively, whereas "total" represents the sum of all five contributions. The yellow bars donate the results directly calculated using observations, whereas the blue bars denote results from the IBM method and the red bars denote results from the TRM method. The error bars are given as the standard deviation of the mean. The ** indicates that the mean contributions calculated by the two methods are significantly different at the 95% confidence level in a two-sample *t* test.

deforestation in midlatitude regions. The reason that net radiation strongly affects the LST change at night is because despite the fact that the incoming shortwave radiation becomes zero, the net longwave radiation is different between the forest and the open land (more discussions on this will be presented in section 3.2). Our finding of the importance of both aerodynamic resistance and heat storage at night is consistent with the study by Schultz et al. (2017), who found that during nighttime rougher forests effectively bring heat aloft down to the surface (i.e., the aerodynamic resistance effect) and forests release the heat stored during the day (i.e., the heat storage effect).

Similar to the results in summer, in winter deforestation also has a warming effect on LST during the daytime (Figure 5), and a cooling effect during the nighttime (Figure 6). Notably, during the daytime in winter, the cooling effect of the radiation term is much greater at pair 4 than its counterpart at the first three paired sites, which could be due to the more frequent snow cover at this location. Overall, the key controlling factors on LST changes due to deforestation are consistent between summer and winter. The LST changes during daytime are mainly caused by changes in aerodynamic resistance (Figures 3 and 5). However, the controlling factors on the nighttime LST changes include albedo, aerodynamic resistance, surface resistance, and heat storage (Figures 4 and 6).

3.2. Similarity and Dissimilarity Between the IBM and TRM Results

At first glance, the results of the two attribution methods seem similar. However, close inspection reveals that the contribution of aerodynamic resistance estimated by the IBM method is generally larger than the contribution estimated by the TRM method, especially when the mean contributions estimated by the two methods are significantly different from each other at the 95% confidence level (indicated by **), for example,

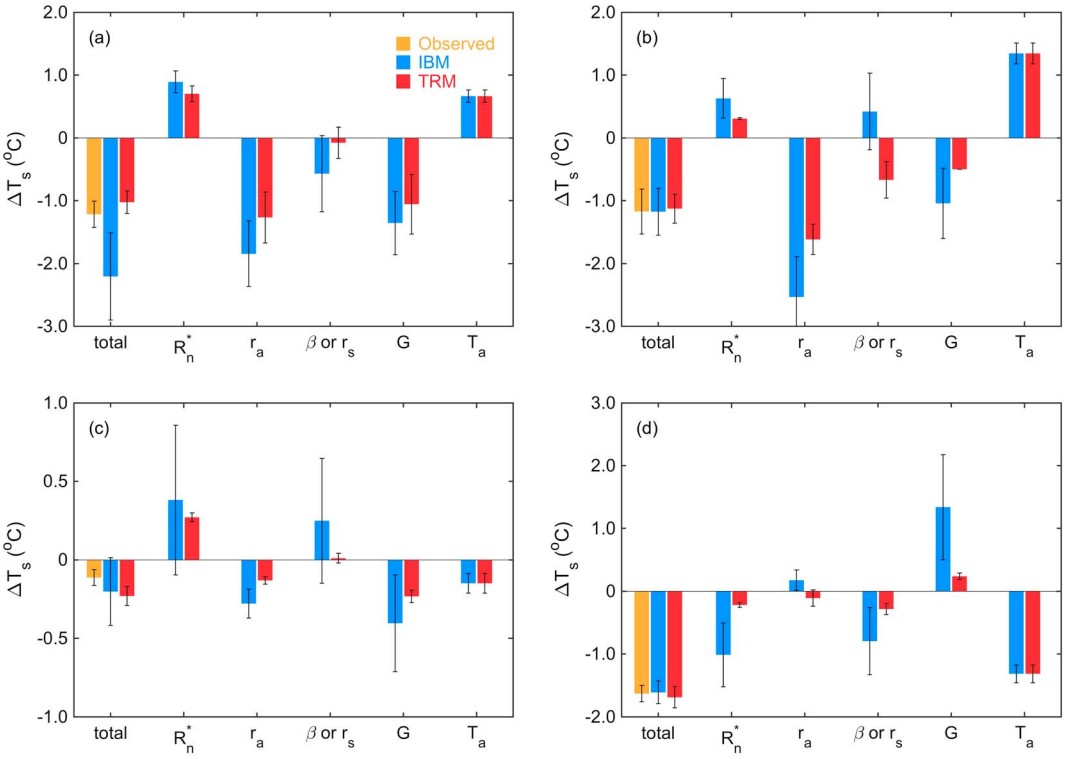

Figure 4. Same as Figure 3 but for the nighttime in summer.

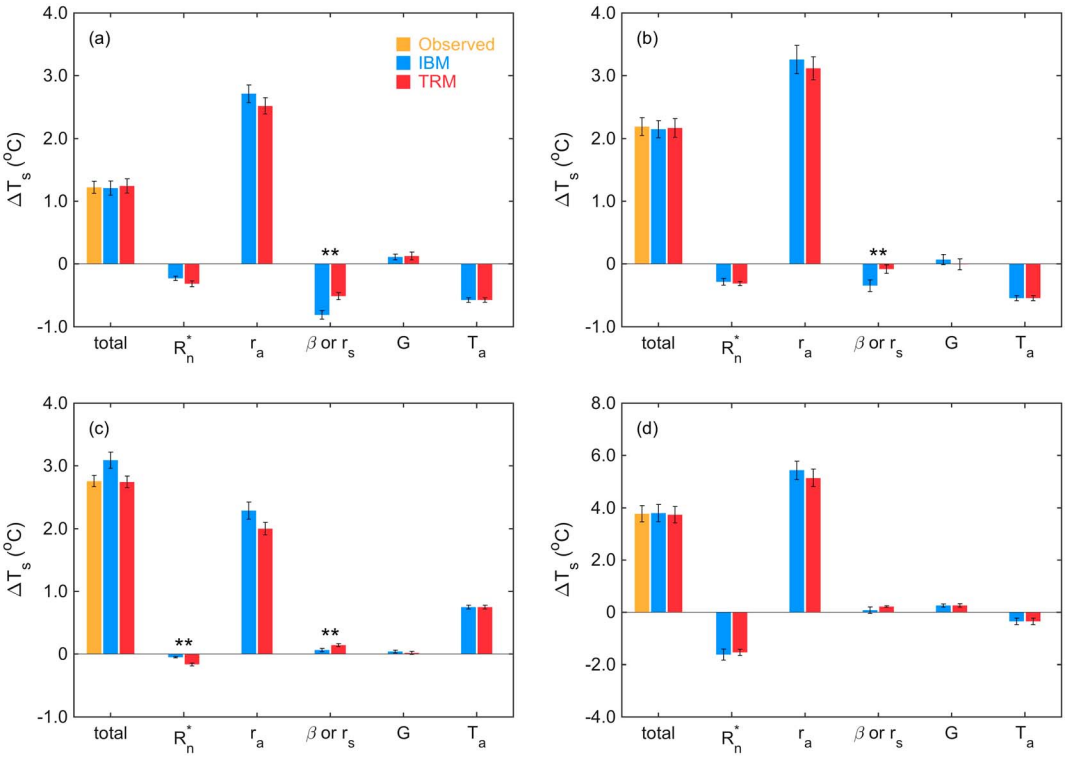

Figure 5. Same as Figure 3 but for the daytime in winter.

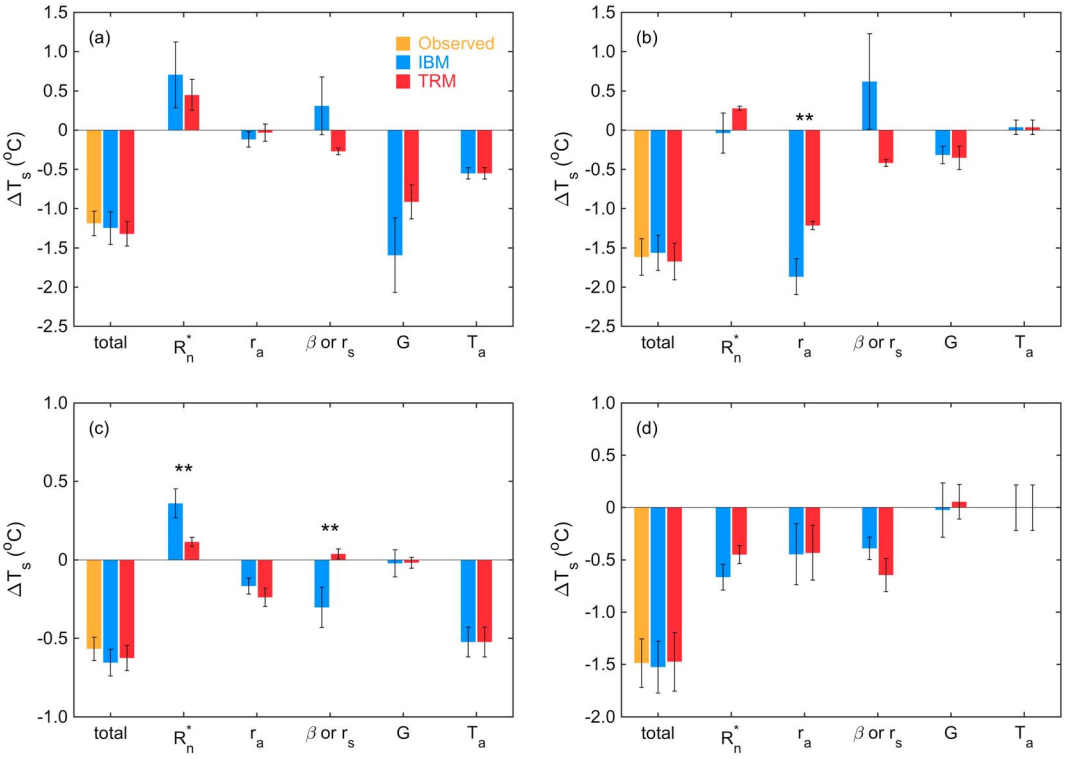

Figure 6. Same as Figure 3 but for the nighttime in winter.

during the daytime in summer at pair 4 (Figure 3d) and during the nighttime in winter at pair 2 (Figure 6b). These results are consistent with the finding of Rigden and Li (2017) that the IBM method tends to overestimate the contribution of the aerodynamic resistance due to the assumption of independence between aerodynamic resistance and Bowen ratio. In addition, Rigden and Li (2017) showed that this overestimation is particularly large in arid regions during daytime in summer and our results support their finding (Figure 3d).

The contributions of the radiation term and the heat storage term are also different between the IBM and TRM method. Compared to the TRM method, the IBM method tends to underestimate the contributions of the radiation term and the heat storage term during the daytime (Figures 3 and 5) and overestimates them during the nighttime (Figures 4 and 6). According to the equations (8) and (13), the contributions of the radiation and heat storage share the same partial derivative or sensitivity, which is $\left(\frac{\partial T_s}{\partial R_n^*}\right)^{\mathrm{IBM}} = \frac{\lambda_o}{1+f_{\mathrm{IBM}}}$ and $\left(\frac{\partial T_s}{\partial R_n^*}\right)^{\mathrm{TRM}} = \frac{\lambda_o}{1+f_{\mathrm{TRM}}}$ in the IBM and TRM methods, respectively. Since the values of ΔR_n^* and ΔG are the same for two methods, the differences are mainly caused by the differences between $\left(\frac{\partial T_s}{\partial R_n^*}\right)^{\mathrm{IBM}}$ and $\left(\frac{\partial T_s}{\partial R_n^*}\right)^{\mathrm{TRM}}$, which are further controlled by the differences in the energy redistribution factor $f_{\mathrm{IBM}} = \frac{r_o}{r_a}\left(1+\frac{1}{\beta}\right)$ and $f_{\mathrm{TRM}} = \frac{r_o}{r_a}\left[1+\frac{\delta}{\gamma}\left(\frac{r_a}{r_a+r_s}\right)\right]$.

To explore the impact of different energy redistribution factors on the estimated contributions of the radiation term and the heat storage term, we compare the values of $1/(1+f)$ at the forest and open land sites during the daytime and nighttime in summer and winter, respectively, as shown in Figures S4–S7. For both the IBM and TRM methods, the values of $1/(1+f)$ at the open land sites are generally larger than those at the forest sites. This reflects the smaller Bowen ratio or larger aerodynamic resistance at the open land sites compared to the forest sites and is consistent with the results in Bright et al. (2017). When the values of $1/(1+f)$ estimated by the two methods are significantly different from each other at the 95% confidence level, those from the IBM method are always smaller than those from the TRM in the daytime, but larger in the nighttime. These patterns are well constrained by physical principles governing evaporation and the Bowen ratio.

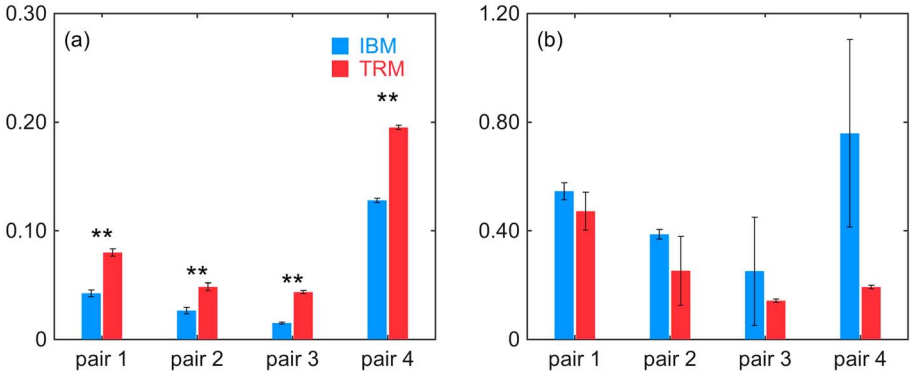

Figure 7. The weighted average of $1/(1 + f)$ for the four pairs during (a) daytime and (b) nighttime in summer. The blue bars denote values calculated by the IBM method, whereas the red bars denote values calculated by the TRM method. The error bars are given as the standard deviation of the mean. The ** indicates that the mean values of $1/(1 + f)$ calculated by the two methods are significantly different at the 95% confidence level in a two-sample *t* test.

According to the upper-bound on the Bowen ratio that forbids supersaturation above an evaporating surface (Philip, 1987), β should be less than γ/δ. Since $(r_a + r_s)/r_a$ is always larger than 1, $1/\beta$ will always be larger than $\frac{\delta}{\gamma}\left(\frac{r_a}{r_a+r_s}\right)$ during the daytime when evaporation is generally positive or upward. Hence $1/(1 + f_{IBM})$ will be smaller than $1/(1 + f_{TRM})$ during the daytime, which agrees well with the observed patterns (Figures S4 and S6). During the nighttime, however, the sensible heat flux is often negative (Figure 1) and the latent heat flux can be either slightly positive or slightly negative. Thus, the physical bounds on the Bowen ratio cannot be used to constrain the difference between the two methods. In this case, we have to only rely on the observations, which show that $1/(1 + f_{IBM})$ tends to be larger than $1/(1 + f_{TRM})$ during the nighttime (Figures S5 and S7). It is noted that $1/(1 + f_{IBM})$ can also be negative during the nighttime (Figure S7).

While the comparison of $\partial T_s/\partial R_n^*$ at each site shows consistent differences between the IBM and TRM methods, the weighted average approach (equation (17)) complicates the comparison slightly. We further estimated the weighted average of $1/(1 + f)$ according to equation (17) for the IBM and TRM methods, respectively (see Figures 7 and 8). It can be seen that when the weighted average of $1/(1 + f)$ from the two methods are significantly different from each other at the 95% confidence level, the one estimated by the IBM is smaller than that estimated by the TRM method during the daytime but larger during the nighttime. These differences in the weighted average of $1/(1 + f)$ between the IBM and TRM methods show good agreement with the differences in the contributions of the radiation term and the heat storage term at the four-paired sites (Figures 3–6). These results indicate that differences in the parameterization of evapotranspiration, which lead to different energy redistribution factors, result in different sensitivities of LST to

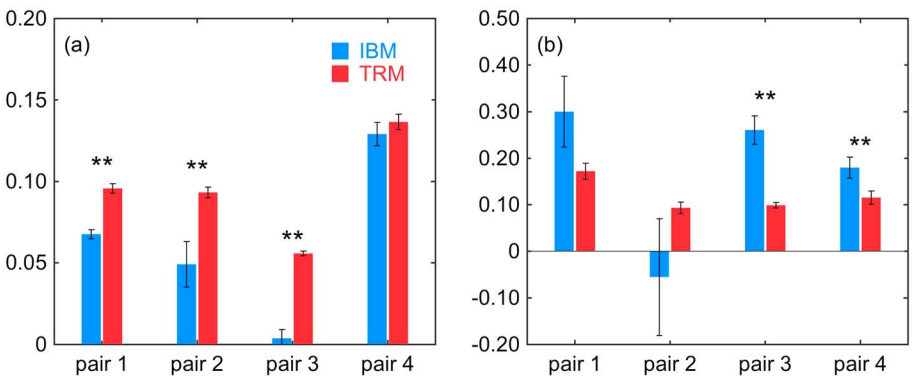

Figure 8. Same as Figure 7 but in winter.

changes in the radiation and heat storage between the two methods. Specifically, the IBM method tends to underestimate the contributions of radiation and heat storage during the daytime but overestimate them during the nighttime.

It is interesting to point out that the contribution of the radiation term is always positive during the nighttime at the first three paired sites, but negative at pair 4 in summer (Figure 4) and winter (Figure 6). According to the formulation $R_n^* = S_{\text{in}}(1-\alpha) + \varepsilon L_{\text{in}} - \varepsilon\sigma T_a^4$, the apparent net radiation is determined by incoming shortwave radiation, incoming longwave radiation, and air temperature. After sunset, the incoming shortwave radiation is nearly zero and the sign of ΔR_n^* should be only affected by the differences of the incoming longwave radiation and air temperature between the forest site and the open land site. In pairs 1 to 3, the values of the incoming longwave radiation at the open land site are larger than those at the forest site during the nighttime in summer (see Figure 1c for pair 1), while the air temperature differences are smaller than or closer to zero (Figures 4a–4c). Therefore, the sign of ΔR_n^* is positive at these three pairs. At pair 4, however, the values of the incoming longwave radiation at the open land site are smaller than those at the forest site during the nighttime in summer (Figure S8c), which results in the negative ΔR_n^*.

4. Conclusions

Using data collected at four paired eddy covariance sites, we explore the impacts of deforestation on LST based on two attribution methods: the IBM and TRM methods. The results of the two methods consistently show that the warming effect on LST induced by deforestation during the daytime is dominated by changes in aerodynamic resistance (mainly depending on the surface roughness) in the northern midlatitudes, but the cooling effect during the nighttime is controlled by changes in albedo, aerodynamic resistance, surface resistance, and heat storage. Both methods also indicate that changes in atmospheric temperature have a large impact on changes in LST and need to be included in the LST attribution.

By comparing the attribution results from the two methods, we find that the assumption underlying the IBM method that the aerodynamic resistance and the Bowen ratio are independent of each other leads to an overestimation of the contribution of aerodynamic resistance to LST change. In addition, the energy redistribution factor in the IBM method is observed to be larger than that in the TRM method in the daytime, but smaller in the nighttime. The larger energy redistribution factor in the IBM method in the daytime results from the upper limit of Bowen ratio over an evaporating surface. As a result, the IBM method underestimates the contribution of albedo and heat storage during the daytime but overestimates them during the nighttime.

We find that both the IBM and TRM methods are sensitive to the temporal scale of attribution, and the higher-order terms neglected in the Taylor expansion. The accuracy of both IBM and TRM methods to estimate daily LST change is improved when the input variables are aggregated to the daily scale. The weighted average approach to compute the partial derivatives further reduces the model uncertainties caused by neglecting higher-order terms in Taylor series expansion.

Both the IBM and TRM methods are based on the surface energy balance equation. As a result, energy balance closure is an important condition for the two models (Wang et al., 2018). Unfortunately, the measured fluxes do not always satisfy the surface energy balance condition and the ground heat flux or heat storage measurements are not always available. In this study, the heat storage is treated as the residual of the surface energy balance equation. While this guarantees surface energy balance, the contribution of the heat storage needs to be carefully interpreted as it also reflects the role of energy imbalance.

Correctly attributing the changes in LST to different biophysical effects is important for improving our understanding of local temperature response to deforestation and designing mitigation strategies. Our study highlights that the outcome depends on the selected attribution method and is very sensitive to how the attribution method is implemented, which partly explains the large uncertainty in our understanding of the impact of deforestation in midlatitude regions. Our study also suggests that acceptable agreement between observed and modeled ΔT_s is the prerequisite for the model to correctly attribute LST change. We recommend that the RMSE of the modeled ΔT_s is reported in future studies that use these attribution methods in order to demonstrate the models' performance in capturing LST changes at the scale that the attribution is performed.

Acknowledgments
We thank the AmeriFlux primary investigators of the sites used in this study. AmeriFlux data are available at http://ameriflux.lbl.gov. This work was conducted when the first author visited Boston University in 2017–2018, which was supported by the National Natural Science Foundation of China (grant 41671398) and the International Program for PhD Candidates at Sun Yat-Sen University.

References

Alkama, R., & Cescatti, A. (2016). Biophysical climate impacts of recent changes in global forest cover. *Science*, *351*(6273), 597–600. https://doi.org/10.1126/science.aad7270

Bonan, G. B. (2008). Forests and climate change: Forcings, feedbacks, and the climate benefits of forests. *Science*, *320*(5882), 1444–1449. https://doi.org/10.1126/science.1155121

Bright, R. M., Davin, E., Halloran, T. O., Pongratz, J., Zhao, K., & Cescatti, A. (2017). Local temperature response to land cover and management change driven by non-radiative processes. *Nature Climate Change*, *7*(4), 296–302. https://doi.org/10.1038/NCLIMATE3250

Bright, R. M., Zhao, K., Jackson, R. B., & Cherubini, F. (2015). Quantifying surface albedo and other direct biogeophysical climate forcings of forestry activities. *Global Change Biology*, *21*(9), 3246–3266. https://doi.org/10.1111/gcb.12951

Burakowski, E., Tawfik, A., Ouimette, A., Lepine, L., Novick, K., Ollinger, S., et al. (2017). The role of surface roughness, albedo, and Bowen ratio on ecosystem energy balance in the eastern United States. *Agricultural and Forest Meteorology*, *249*, 367–376. https://doi.org/10.1016/j.agrformet.2017.11.030

Cao, C., Lee, X., Liu, S., Schultz, N., Xiao, W., Zhang, M., & Zhao, L. (2016). Urban heat islands in China enhanced by haze pollution. *Nature Communications*, *7*, 1–7. https://doi.org/10.1038/ncomms12509

Chen, L., & Dirmeyer, P. A. (2016). Adapting observationally based metrics of biogeophysical feedbacks from land cover/land use change to climate modeling. *Environmental Research Letters*, *11*(3). https://doi.org/10.1088/1748-9326/11/3/034002

Davin, E. L., & De Noblet-Ducoudre, N. (2010). Climatic impact of global-scale deforestation: Radiative versus nonradiative processes. *Journal of Climate*, *23*(1), 97–112. https://doi.org/10.1175/2009JCLI3102.1

Defries, R. S., Bounoua, L., & Collatz, G. J. (2002). Human modification of the landscape and surface climate in the next fifty years. *Global Change Biology*, *8*(5), 438–458. https://doi.org/10.1046/j.1365-2486.2002.00483.x

Dore, S., & Kolb T. (2016a). AmeriFlux US-Fmf Flagstaff—Managed forest from 2006–2010. https://doi.org/10.17190/AMF/1246050

Dore, S., & Kolb T. (2016b). AmeriFlux US-Fwf Flagstaff—Wildfire from 2006–2010. https://doi.org/10.17190/AMF/1246052

Feddema, J. J., Oleson, K. W., Bonan, G. B., Mearns, L. O., Buja, L. E., Meehl, G. A., & Washington, W. M. (2005). The importance of land-cover change in simulating future climates. *Science*, *310*(5754), 1674–1678. https://doi.org/10.1126/science.1118160

Findell, K. L., Berg, A., Gentine, P., Krasting, J. P., Lintner, B. R., Malyshev, S., et al. (2017). The impact of anthropogenic land use and land cover change on regional climate extremes. *Nature Communications*, *8*(1), 989. https://doi.org/10.1038/s41467-017-01038-w

Intergovernmental Panel on Climate Change (2013). *Climate change 2013: The physical science basis*. Cambridge, UK: Cambridge University Press.

Juang, J. Y., Katul, G., Siqueira, M., Stoy, P., & Novick, K. (2007). Separating the effects of albedo from eco-physiological changes on surface temperature along a successional chronosequence in the southeastern United States. *Geophysical Research Letters*, *34*, L21408. https://doi.org/10.1029/2007GL031296

Lee, X., Goulden, M. L., Hollinger, D. Y., Barr, A., Black, T. A., Bohrer, G., et al. (2011). Observed increase in local cooling effect of deforestation at higher latitudes. *Nature*, *479*(7373), 384–387. https://doi.org/10.1038/nature10588

Li, Y., De Noblet-Ducoudré, N., Davin, E. L., Motesharrei, S., Zeng, N., Li, S., & Kalnay, E. (2016). The role of spatial scale and background climate in the latitudinal temperature response to deforestation. *Earth System Dynamics*, *7*(1), 167–181. https://doi.org/10.5194/esd-7-167-2016

Li, Y., Zhao, M., Motesharrei, S., Mu, Q., Kalnay, E., & Li, S. (2015). Local cooling and warming effects of forests based on satellite observations. *Nature Communications*, *6*(1), 6603. https://doi.org/10.1038/ncomms7603

Luyssaert, S., Jammet, M., Stoy, P. C., Estel, S., Pongratz, J., Ceschia, E., et al. (2014). Land management and land-cover change have impacts of similar magnitude on surface temperature. *Nature Climate Change*, *4*(5), 389–393. https://doi.org/10.1038/nclimate2196

Mahmood, R., Pielke, R. A., Hubbard, K. G., Niyogi, D., Paul, A., Mcalpine, C., et al. (2014). Land cover changes and their biogeophysical effects on climate. *International Journal of Climatology*, *34*(4), 929–953. https://doi.org/10.1002/joc.3736

Monteith, J. L., & Unsworth, M. H. (1990). *Principles of environmental physics*. London, UK: Edword Arnold.

Noormets, A. (2016a). AmeriFlux US-NC1 NC_Clearcut from 2005–2013. https://doi.org/10.17190/AMF/1246082

Noormets, A. (2016b). AmeriFlux US-NC2 NC_Loblolly Plantation from 2005–present. https://doi.org/10.17190/AMF/1246083

Oishi, C., Novick, K., & Stoy, P. (2016a). AmeriFlux US-Dk1 Duke Forest-open field from 2001–2008. https://doi.org/10.17190/AMF/1246046

Oishi, C., Novick, K., & Stoy, P. (2016b). AmeriFlux US-Dk2 Duke Forest-hardwoods from 2001–2008. https://doi.org/10.17190/AMF/1246047

Oishi, C., Novick, K., & Stoy, P. (2016c). AmeriFlux US-Dk3 Duke Forest-loblolly pine from 2001–2008. https://doi.org/10.17190/AMF/1246048

Philip, J. R. (1987). A physical bound on the Bowen ratio. *Journal of Applied Meteorology*, *26*(8), 1043–1045. https://doi.org/10.1175/1520-0450(1987)026%3C1043:APBOTB%3E2.0.CO;2

Pielke, R. A., Pitman, A., Niyogi, D., Mahmood, R., Mcalpine, C., Hossain, F., et al. (2011). Land use/land cover changes and climate: Modeling analysis and observational evidence. *Wiley Interdisciplinary Reviews: Climate Change*, *2*(6), 828–850. https://doi.org/10.1002/wcc.144

Priestley, C. H. B., & Taylor, R. J. (1972). On the assessment of surface heat flux and evaporation using large scale parameters. *Monthly Weather Review*, *100*(2), 81–92. https://doi.org/10.1175/1520-0493(1972)100%3C0081:OTAOSH%3E2.3.CO;2

Rigden, A. J., & Li, D. (2017). Attribution of surface temperature anomalies induced by land use and land cover changes. *Geophysical Research Letters*, *44*, 6814–6822. https://doi.org/10.1002/2017GL073811

Rigden, A. J., Li, D., & Salvucci, G. D. (2017). Dependence of thermal roughness length on friction velocity across land cover types: A synthesis analysis using AmeriFlux data. *Agricultural and Forest Meteorology*, *249*, 512–519. https://doi.org/10.1016/j.agrformet.2017.06.003

Rigden, A. J., & Salvucci, G. D. (2015). Evapotranspiration based on equilibrated relative humidity (ETRHEQ): Evaluation over the continental U.S. *Water Resources Research*, *51*, 2951–2973. https://doi.org/10.1002/2014WR016072

Rotenberg, E., & Yakir, D. (2011). Distinct patterns of changes in surface energy budget associated with forestation in the semiarid region. *Global Change Biology*, *17*(4), 1536–1548. https://doi.org/10.1111/j.1365-2486.2010.02320.x

Runyan, C. W., D'odorico, P., & Lawrence, D. (2012). Physical and biological feedbacks of deforestation. *Reviews of Geophysics*, *50*, RG4006. https://doi.org/10.1029/2012RG000394

Schultz, N. M., Lawrence, P. J., & Lee, X. (2017). Global satellite data highlights the diurnal asymmetry of the surface temperature response to deforestation. *Journal of Geophysical Research: Biogeosciences*, *122*, 903–917. https://doi.org/10.1002/2016JG003653

Tao, Z., Santanello, J. A., Chin, M., Zhou, S., Tan, Q., Kemp, E. M., & Peters-Lidard, C. D. (2013). Effect of land cover on atmospheric processes and air quality over the continental United States-a NASA Unified WRF (NU-WRF) model study. *Atmospheric Chemistry and Physics*, *13*(13), 6207–6226. https://doi.org/10.5194/acp-13-6207-2013

Wang, L., Lee, X., Schultz, N., Chen, S., Wei, Z., Fu, C., et al. (2018). Response of surface temperature to afforestation in the Kubuqi Desert, Inner Mongolia. *Journal of Geophysical Research: Atmospheres*, *123*, 948–964. https://doi.org/10.1002/2017JD027522

Zhao, L., Lee, X., & Schultz, N. M. (2017). A wedge strategy for mitigation of urban warming in future climate scenarios. *Atmospheric Chemistry and Physics*, *17*(14), 9067–9080. https://doi.org/10.5194/acp-17-9067-2017

Zhao, L., Lee, X., Smith, R. B., & Oleson, K. (2014). Strong contributions of local background climate to urban heat islands. *Nature*, *511*(7508), 216–219. https://doi.org/10.1038/nature13462